CoGa Catalysts for the Hydrogenation of CO_2 to Methanol

Joseph A. Singh,[1] Ang Cao,[2,3], Julia Schumann, [2,3] Tao Wang, [2,3] Jens K. Nørskov,[2,3] Frank Abild-Pedersen,[2,3] and Stacey F. Bent[3]

1. Department of Chemistry, Stanford University, 333 Campus Drive, Stanford, California, 94305, USA
2. SUNCAT Center for Interface Science and Catalysis, SLAC National Accelerator Laboratory, 2575 Sand Hill Road, Menlo Park, CA 94025, USA
3. SUNCAT Center for Interface Science and Catalysis, Department of Chemical Engineering, Stanford University, 443 Via Ortega, Stanford, California, 94305, USA

Abstract

Methanol is an important chemical compound which is used both as a fuel and as a platform molecule in chemical production. Synthesizing methanol, as well as dimethyl ether, directly from carbon dioxide and hydrogen produced using renewable electricity would be a major step forward in enabling an environmentally sustainable economy. We utilize density functional theory combined with microkinetic modeling to understand the methanol synthesis reaction mechanism on a model CoGa catalyst. A series of catalysts with varying Ga content are synthesized and experimentally tested for catalytic performance. The performance of these catalysts is sensitive to the Co:Ga ratio, whereby increased Ga content resulted in increased methanol and dimethyl ether selectivity and increased Co content resulted in increased selectivity towards methane. We find that the most active catalysts have up to 95% CO-free selectivity towards methanol and dimethyl ether during CO_2 hydrogenation and are comparable in performance to a commercial CuZn catalyst. Using *in*-situ DRIFTS we experimentally verify the presence of surface formate during CO_2 hydrogenation in support of our theoretical calculations.

Introduction

From carbon dioxide and hydrogen, methanol can be synthesized and used as a versatile molecule to store energy and as a platform molecule for chemical production.[1] If the hydrogen is produced using renewable electricity, this route to methanol could represent an important step in a sustainable carbon cycle. Currently 70 million tonnes per year of methanol are produced, and methanol is already an important component for polymer production and used as a fuel additive. Commercial methanol production uses syngas produced from fossil sources and catalysts consisting of Cu and ZnO supported on Al_2O_3.[2] By utilizing CO_2 a carbon negative process based on CO_2 capture can be devised.

Recent work has discovered a Ni/Ga-based intermetallic material as a promising new catalyst that behaves differently than the conventional Cu-based catalyst used for CO_2 hydrogenation to methanol.[3,4] Ga has also shown promise as a promoter for Cu-based methanol synthesis catalysts.[5,6] In the present work we show that the combination of Co and Ga is also a good catalyst for CO_2 hydrogenation to methanol. Recent work has reported that CoGa catalysts have a significant selectivity towards higher alcohols during CO hydrogenation.[7,8] However, no prior reports have considered CoGa for the hydrogenation of CO_2 to methanol.

In this work, we applied a descriptor-based approach and micro kinetic modeling on different metal surfaces to simulate the catalytic performance of methanol synthesis from CO_2 and H_2. Based on the descriptors, a class of CoGa catalysts were identified as active and selective towards methanol formation. To test the descriptor-based result, we explicitly performed Density Functional Theory (DFT) calculations on the reaction intermediates in the CO_2 hydrogenation process for CoGa and used this data to identify plausible reaction mechanisms and analyze activity/selectivity relationships. We performed experimental synthesis and characterization of CoGa catalysts to explore the effects of catalyst composition on performance. We discovered that CoGa catalysts exhibit up to 95% CO free selectivity to methanol and dimethyl ether.

Methods

Computational Methods

All calculations were carried out using the Quantum Espresso software[9] interfaced with the Atomic Simulation Environment (ASE).[10] The BEEF-vdW[11] exchange correlation functional was used because of its accurate estimation of adsorption energies[12] and its explicit inclusion of van der Waals interactions. The nudged elastic band (NEB)[13] method was used to identify transition-state structures and their energies. All calculations were performed with a plane-wave cutoff of 500 eV, a density cutoff of 5000 eV, and a Monkhorst-Pack type k-point sampling of 4×4×1.

A four layer (2×4) bcc (110) slab was used in the calculations with the top two layers allowed to relax during the geometric optimizations until the force on each atom was less than 0.03 eV/Å. The slabs were separated by at least 15 Å of vacuum in the (110) direction. Dipole correction was included in all cases to decouple the electrostatic interaction between periodically repeated slabs.

Microkinetic modeling was carried out using the CatMAP software package.[14] Rates were determined by numerically solving the coupled differential equations with the steady state approximation.

Selectivity was defined as the rate of formation of the product of interest divided by the rates of formation for methane, methanol, and CO without any weighting for the number of carbons. In this work, surfaces were modeled using two surface sites: a "hydrogen reservoir" site and a site for all other intermediates as done in previous work.[15] Further details and all numerical inputs to the kinetic model can be found in previous work.[16,17]

For a fast screening of possible catalyst candidates, a one-descriptor model was used based on work by Studt et al.[4] Electronic energies and zero point energy corrections for the 1D volcano plot as well as the enthalpy and entropy corrections were taken from Studt et al.[4]

Catalyst Synthesis and Characterization

Catalysts were synthesized via incipient wetness impregnation (IWI). $Co(NO_3)_2*6H_2O$ (Aldrich) and $Ga(NO_3)_3*xH_2O$ (Aldrich) were dissolved in deionized water. The metal salt mass was chosen to have 16 weight percent total metal content in the catalyst. The solution was added to degassed silica gel (Davisil 643, Aldrich). Catalysts were dried at 80 °C for 15 hours. Catalysts were subsequently reduced in H_2 by heating to 700 °C at 5 °C/minute then holding for 2 hours.

Co catalysts supported on silica gel were synthesized likewise via IWI to yield catalysts with 10 weight % Co metal loading. The Co catalysts were dried at room temperature and then calcined at 350 °C in air.

ICP-OES was performed using a Thermo Fisher ICAP 6300 Duo View ICP-OES spectrometer. Samples were first digested in hot nitric acid (TraceMetal Grade, Fischer). Elemental standards were obtained from Aldrich and diluted with deionized water.

Nitrogen physisorption measurements were performed with a Micromeritics 3 Flex instrument. Surface areas were calculated using the Brunauer-Emmett-Teller (BET) method. Pore volumes were calculated using the Barett-Joyner-Halenda (BJH) method.

Powder X-ray diffraction was performed using a Bruker D8 diffractometer with Mo k-alpha source. Samples were measured in 1 mm quartz capillaries.

TEM was performed using a FEI Tecnai and FEI Titan microscopes operating in brightfield mode. Catalysts were dropcast from ethanol onto TEM grids (TedPella). Scanning transmission electron microscopy (STEM) and energy dispersive spectroscopy (EDS) were performed on the FEI Titan microscope. STEM-EDS line scans were smoothed using 4 point moving window average.

In-situ diffuse reflectance infrared Fourier transform spectroscopy (DRIFTS) was performed using a previously-described custom instrument.[18] Catalysts were reduced in H_2 at 450 °C for 1 hour. A background spectrum of a catalyst was acquired after reduction. The catalyst was then pressurized to 9 bar in flowing 3:1 H_2:CO_2 at 250 °C. Spectra were acquired once the pressure stabilized in a 3:1 H_2:CO_2 flow.

Catalyst performance was evaluated using an Altamira Benchcat 4000 HP reactor. In each measurement, a catalyst was packed into a bed between plugs of quartz wool in a 0.25 inch outer diameter Silcolloy (SilcoTek) coated stainless steel tube. The catalyst was reduced at 450 °C for 1 hour in H_2. Catalysts were heated to the desired reaction temperature and pressurized in 3:1 H_2:CO_2. Products were quantified using an online Agilent 7890B gas chromatograph-mass spectrometer (GCMS). Hydrocarbon products were quantified using a flame ionization detector and carbon monoxide using a thermal conductivity detector. Testing was performed under differential conditions.

A commercial CuZn methanol synthesis catalyst was used for comparison from Alfa Aesar. The catalyst's primary components are CuO, ZnO, Al_2O_3, and MgO as reported by the manufacturer. The catalyst pellets were ground using a mortar and pestle and tested as described above.

Results and Discussion

CoGa Catalyst Discovery and Mechanism

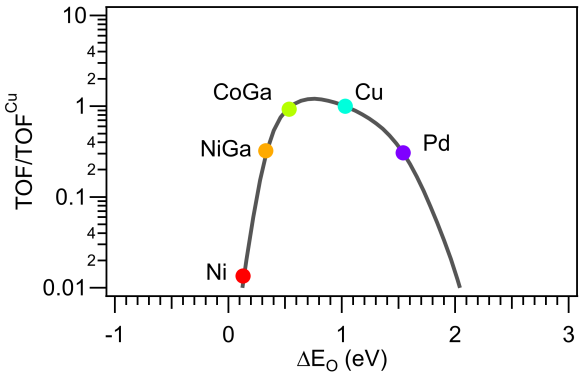

Figure 1. Calculated turnover frequencies (TOF) relative to copper (TOF^{Cu}) as a function of oxygen (ΔE_O) binding energies. Calculations were performed for 250 °C with 6.67 bar carbon dioxide, 23.33 bar hydrogen, 0.01 bar water, and 0 bar methane, methanol, and carbon monoxide.

In our analysis, we combined DFT calculations and microkinetic modelling to study CO_2 hydrogenation on metal surfaces. We have used energy scaling relations to describe reaction and transition-state energies for the CO_2 hydrogenation reaction network in terms of carbon monoxide and oxygen binding energies only in accordance with prior work.[4,19] We used a volcano generated from this approach by Studt et al. to perform an initial screening.[4] The volcano allows for estimating the turn over frequency (TOF) of methanol synthesis as a function of O binding energy and the results of performing this analysis are presented in Figure 1.

As can be seen in Figure 1, the calculated value of O binding energy on CoGa is located in the region of high methanol activity. CoGa is expected to have reasonable activity towards methanol, comparable to monometallic Cu. This suggests that CoGa could be a good catalyst candidate for methanol synthesis.

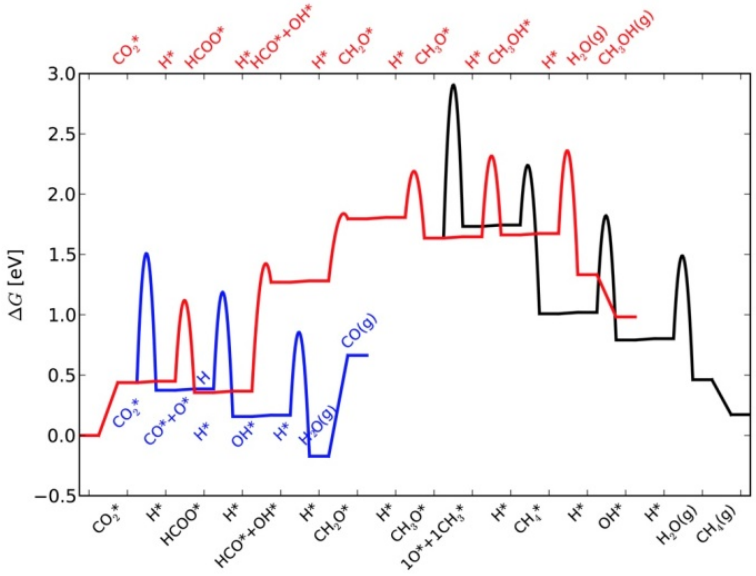

Figure 2. Free energy diagrams of methane (black), methanol (red), and carbon monoxide (blue) formation at 250 °C on the Co_1Ga_1 (110) surface. Free energies of reactants (CO_2, H_2) are calculated for 30 bar 3:1 H_2:CO_2. All other free energies are computed at the standard state.

In the following, we used DFT to investigate the CoGa catalyst in more detail. We performed explicit calculations of reaction and activation energies for the pathway of CO_2 hydrogenation to methanol on the Co_1Ga_1 (110) surface. Co_1Ga_1 has a BCC crystal structure and we chose the stable close-packed (110) surface as our model structure. The calculated reaction energies and barriers of elementary reactions involved in the formation of methane, methanol, and carbon monoxide are presented in Table S1 and from this we identified the most favorable pathways for methane, methanol, and CO formation. Similar to NiGa[4] and CuZnO[20], we found that methanol is formed via a formate pathway. Compared with NiGa,

the hydrogenation of formate on CoGa proceeds via a modified pathway where the C-OH bond of HCOOH was split rather than H_2COOH as in the case of NiGa.[4]

To form hydrocarbons, such as methane, we found that the most energetically favorable pathway required splitting of the C-O bond in the CH_3O intermediate. The CH_3O intermediate splitting had a barrier of 1.40 eV whereas the barrier to hydrogenate CH_3O to CH_3OH was only 0.75 eV. This indicated that CoGa would form methanol rather than methane or any other hydrocarbons in which the C-O bond split in CH_3O is required.

The most favorable way to form CO was via the direct reverse water gas shift pathway, not involving a formate intermediate (Figure 2). In this process CO_2(g) directly splits to CO^* and O^* with the CO^* being desorbed as CO(g) and the O^* reacting with H^* forming H_2O(g).

Based on the energetics shown in the free energy diagram in Figure 2, there is a competition between dissociation of CO_2^* to CO, and the hydrogenation step to form HCOO*. These two steps are critical in determining the overall product selectivity. As CO_2 hydrogenation is a complex multistep process, we performed microkinetic modelling to make quantitative predictions of the overall activity and selectivity.

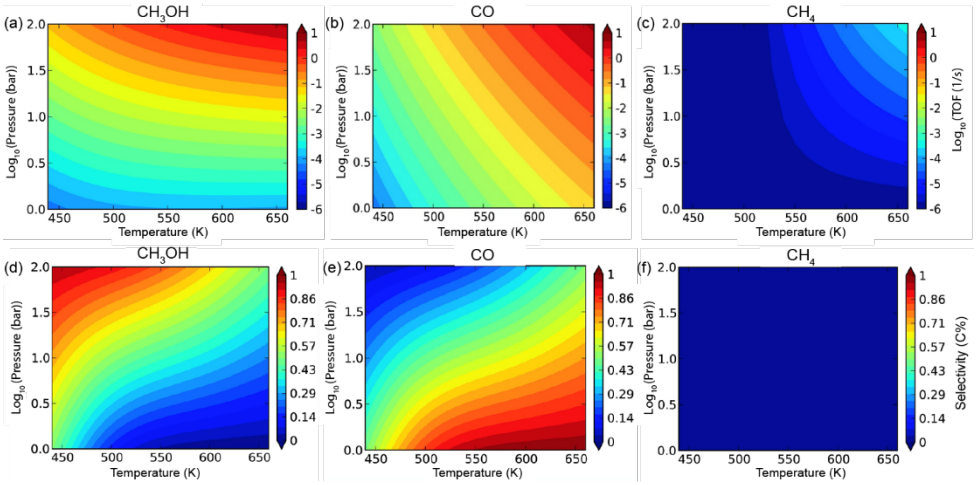

Figure 3. Calculated turnover frequencies (TOF) as a function of temperature and pressure for methanol (a), carbon monoxide (b), and methane (c), and corresponding selectivities (d-f) on Co_1Ga_1 (110). Modelling was performed under the conditions of 3:1 H_2:CO_2, 0.01 bar water, and 0 bar methane, methanol, and carbon monoxide.

The activity and selectivity for methanol, carbon monoxide, and methane formation calculated as a function of temperature and pressure are presented in Figure 3. The rate of methane formation was

Frank
Delete

Frank
Delete

Frank
Delete

much lower than that of the other two products due to the higher barrier for splitting the C-O bond in CH_3O^*. Therefore, the methane selectivity would be very low on the Co_1Ga_1 (110) surface

At low temperatures, a higher activity and selectivity for methanol over carbon monoxide formation was observed. With increasing temperature, the rate of carbon monoxide formation increased faster than the rate of methanol formation. Thus, the selectivity for methanol decreased, while the selectivity for CO increased. Methanol, therefore, would be the primary product on Co_1Ga_1 (110) surface at lower temperatures, and CO would be more favorable at higher temperatures.

CoGa Catalyst Characterization and Evaluation

To test the computational predictions, CoGa catalysts were synthesized and experimentally evaluated. The elemental composition of the catalyst, surface area, and porosity are presented in Table 1. A variety of compositions were considered as our computational predictions refer to a surface composition and in practice the surface structure and composition of a catalyst can deviated from the bulk composition and structure. The elemental composition of each catalyst closely matched the expected ratio based on the mass of Co and Ga precursors used in each catalyst's synthesis. The prepared catalysts had similar surface areas and porosities, with the Co_5Ga_1 catalyst having slightly lower surface area and porosity.

Table 1. Co/Ga molar ratios, BET surface areas, and BJH pore volumes of CoGa Catalysts

	Co/Ga molar ratio expected	**Co/Ga molar ratio experimental***	**BET Surface Area (m^2/g)**	**BJH Pore Volume (cm^3/g)**
Co_5Ga_1	5.00	5.07	240	0.84
Co_5Ga_3	1.67	1.73	290	1.0
Co_1Ga_1	1.00	1.07	300	1.0

*Calculated using values from ICP-OES

X-ray diffraction (XRD) was used to determine the structure of the catalysts. Based on these results, we can compare the structure of the synthesized catalysts with the structures used in our DFT calculations. XRD patterns of Co_5Ga_1, Co_5Ga_3, and Co_1Ga_1 catalysts are presented in Figure 4. The Co_5Ga_1 catalyst was in a FCC Co phase (PDF Card 00-015-0806). The peaks were shifted relative to those of Co towards smaller 2θ angles. Ga has a larger atomic radius than Co and its incorporation into the FCC Co lattice would result in lattice expansion and thus a shift to smaller 2θ angles.

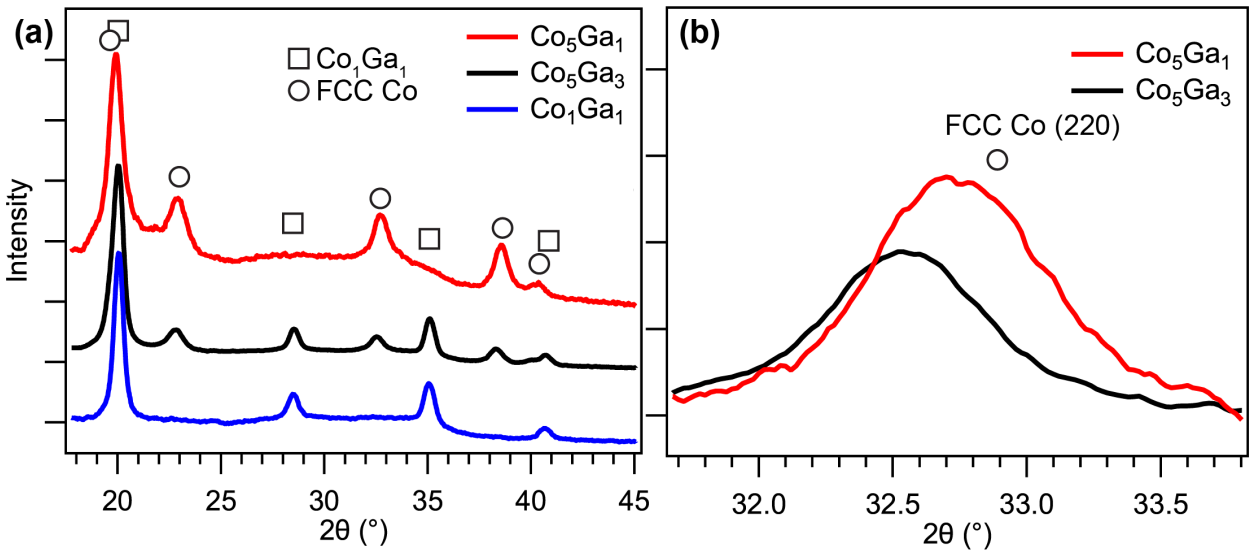

Figure 4. Measured XRD patterns of Co_5Ga_1, Co_5Ga_3, and Co_1Ga_1 catalysts (a). In (b), the FCC Co (220) peaks from (a) are shown with the position of the FCC Co (220) reflection marked with a circle.

The Co_5Ga_3 catalyst had peaks due to both Co_1Ga_1 (PDF 04-001-3339) and FCC Co phases. The FCC Co peaks were further shifted towards smaller 2θ angles than in the Co_5Ga_1 catalyst. The emergence of a Co_1Ga_1 phase and further shifting of the FCC Co peaks agree with the greater Ga content of this catalyst. The Co_1Ga_1 catalyst had no detectable FCC Co peaks and only contained peaks corresponding to a Co_1Ga_1 alloy phase. The sole presence of a Co_1Ga_1 alloy phase agrees with the catalyst stoichiometry. The XRD results support a successful synthesis of alloyed CoGa catalysts.

TEM characterization was used to investigate the structure of the catalysts at the nanoscale, in particular to determine whether the surface is an alloy structure or there is segregation of Co and Ga. We investigated the Co_5Ga_3 catalyst due to its comparatively high activity and selectivity for methanol which will be discussed in the subsequent sections. TEM characterization of the Co_5Ga_3 catalyst after reduction is presented in Figure 5. The catalyst primarily consisted of CoGa domains with the observance of lattice fringes corresponding to a Co_1Ga_1 crystal structure (Figure 5a) in agreement with the XRD results. Based on the imaging, the catalyst had a particle size distribution of 17 ± 4 nm (Figure S1). Elemental analysis of an individual catalyst nanoparticle using STEM-EDS (Figure 5b) indicated a uniform distribution of Co and Ga without evidence for segregation of either species. Elemental mapping of the catalyst over the region shown in Figure 5c is presented in Figure 5d. The majority of the Co and Ga signals were colocalized in nanoparticles. Some Co and Ga signals were observed in parts of the mapping without a clear nanoparticle present. We attributed these signals to noise as similar signals are present in regions of the mapping where no sample was present when correlating with the dark field

Frank Delete
Frank Delete
Frank Delete
Frank Delete
Frank Delete

STEM image (Figure 5c). The TEM results indicated the catalyst has no significant segregation of Co and Ga. The combined XRD and TEM results demonstrated the formation of alloyed CoGa catalysts. Since we successfully formed CoGa catalysts, we can use these catalysts to evaluate our computational predictions for CoGa catalysts.

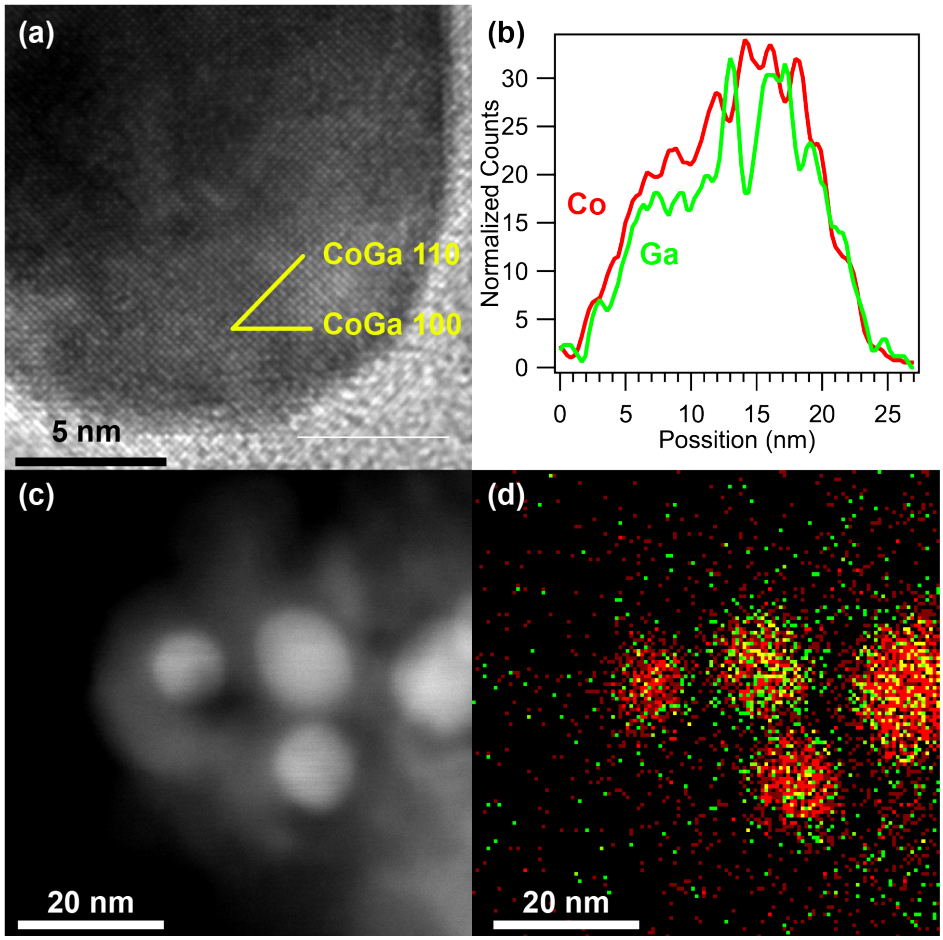

Figure 5. Micrographs and microanalysis of Co_5Ga_3 catalysts. (a) brightfield TEM micrograph, (b) STEM-EDS line scan, and (c) STEM darkfield micrograph and (d) corresponding STEM-EDS elemental mapping with Co in red and Ga in green.

Catalytic Performance

Based on the characterization results, it is evident that we successfully synthesized CoGa catalysts for comparison with our calculated predictions. CoGa catalysts with the compositions characterized above were evaluated for CO_2 hydrogenation performance and the results are presented in Table 2. Methanol was the major product for all catalyst compositions followed by carbon monoxide, while hydrocarbons were trace products with no hydrocarbons heavier than propane detected. The Co_5Ga_3 catalyst had the highest selectivity for methanol. The decrease in methanol selectivity from Co_5Ga_3 to Co_1Ga_1 closely

correlated with an increased selectivity for dimethyl ether between these two catalysts. As shown in Table 2, the increase in dimethyl ether (DME) formation tracked the ratio of Co:Ga, with increasing amounts of Ga correlated with increased DME formation. Dimethyl ether formation is known to occur by the bimolecular dehydration of methanol.[1] The reaction is catalyzed by solid acids such as γ-Al_2O_3.[1] Prior work using pyridine chemisorption found that the addition of Ga_2O_3 increases the acidity of SiO_2.[21] Hence, we speculate that with increasing amounts of Ga, gallium oxide sites may form that catalyze DME formation due to their acidic nature. Because DME formation most likely occurs on sites not related to the CoGa surfaces and is formed through a secondary reaction from methanol product, dimethyl ether formation was not considered in our theoretical calculations. Further, when comparing our calculations with experimental results, DME will be treated as methanol produced by CoGa.

Table 2. Catalytic performance of prepared CoGa catalysts tested at 250°C using 30 bar 3:1 H_2:CO_2

	Selectivity (C%)						
	MeOH	CH_4	HC*	CO	DME**	MeOH + DME CO Free Selectivity	Activity***
Co_5Ga_1	62%	9%	1%	27%	1%	86%	0.19
Co_5Ga_3	63%	4%	0.1%	26%	7%	95%	0.12
Co_1Ga_1	50%	1%	1%	27%	22%	97%	0.06

*ethane and propane **dimethyl ether ***µmol C/g catalyst/s

In addition to differences in DME selectivity, the catalysts showed different selectivities toward methane. The relatively higher methane selectivity on the Co_5Ga_1 catalyst may be the result of isolated Co sites on this Co-rich catalyst since Co has a high methanation activity.[22] The overall high selectivity towards methanol and its secondary product DME agrees with our prediction that CoGa catalysts will exhibit good selectivity toward methanol during CO_2 hydrogenation.

Table 2 shows that with increasing Co content, the activity of the prepared catalysts increased. The exact origin of this behavior is unclear. One possible explanation is that Co-sites are the relevant ones for CO_2 hydrogenation. In catalysts with high Ga content there would be less exposed Co sites due to a reduction in Co content and excess Ga covering surface Co sites. With increasing Co content there would be more active sites and therefore higher activity.

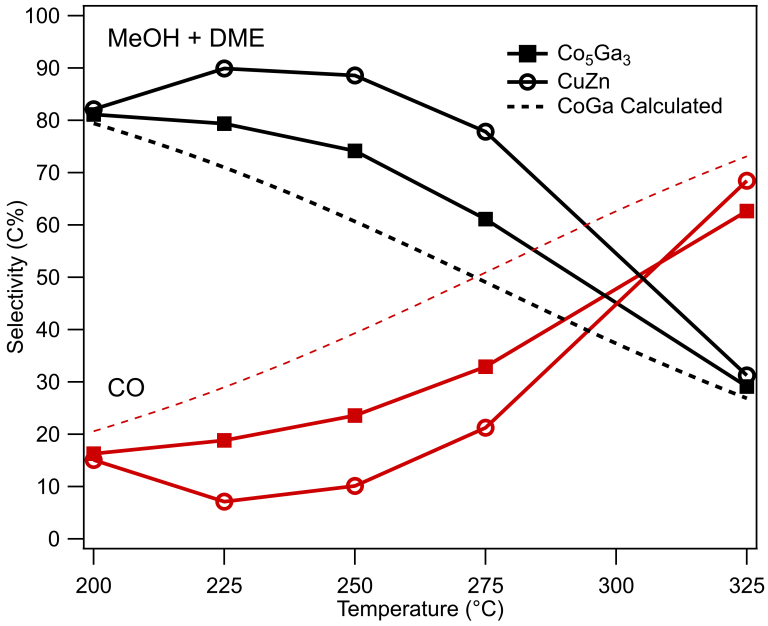

Figure 6. Selectivity of Co_5Ga_3 catalyst (squares) and a commercial CuZn methanol synthesis catalyst (circles) during CO_2 hydrogenation as a function of temperature. The calculated selectivities from Figure 3 are shown as dashed lines.

Frank
Delete

Selectivities of Co_5Ga_3 and a commercial CuZn catalyst are compared in Figure 6. As temperature increased, the Co_5Ga_3 catalyst showed an overall trend of decreasing selectivity towards methanol and dimethyl ether and increasing selectivity towards CO in agreement with our calculations. Although at higher temperatures, the commercial CuZn catalyst had higher selectivity for the desired methanol and dimethyl ether products than did our Co_5Ga_3 catalyst, at 200 °C the selectivity of the Co_5Ga_3 catalyst closely matched that of the commercial CuZn methanol synthesis catalyst. Noting that the commercial CuZn catalyst was highly optimized, we conclude that Co_5Ga_3 is highly promising as laboratory-synthesized catalyst since even unoptimized, it can reach similar performance levels to the commercial catalysts. Moreover, the predicted methanol and CO selectivity closely matched that of the Co_5Ga_3 catalyst. The calculations were performed on a Co_1Ga_1 (110) surface while a real catalyst will contain other surface structures. The discrepancy between the calculated and experimental values most likely resulted from the calculations only considering the Co_1Ga_1 (110) surface.

To investigate the surface chemistry under conditions similar to the operating conditions and verify that formate is present as we predicted theoretically, *in-situ* DRIFTS was performed at 9 bar in flowing 3:1 H_2:CO_2 for Co and Co_5Ga_3 catalysts. The results are presented in Figure 7. Gas phase CO_2, CO, H_2O, and CH_4 species were observed. Much higher CO, H_2O, and CH_4 signals were observed for Co than for Co_5Ga_3 (Figure 7a), in agreement with the low methane and CO selectivity of Co_5Ga_3. In the formate

stretching region of Co_5Ga_3 a peak was observed at 1613 cm^{-1}. Prior work studying CO_2 hydrogenation on Co/Al_2O_3 catalysts assigned a peak at 1597 cm^{-1} to formate on Co during CO_2 hydrogenation.[23] A formate peak at 1595 cm^{-1} was observed on Cu/SiO_2 catalysts during CO_2 hydrogenation.[24] A formate peak at 1583 cm^{-1} was observed on Ni/SiO_2 catalysts during formic acid decomposition.[24] The observed peak on the Co_5Ga_3 catalyst was shifted towards higher frequencies than reported for formate on Co, Cu, and Ni. Ga has a lower electronegativity than Co, Ni, and Cu and therefore a higher formate stretching frequency would be expected for a CoGa alloy than for the pure metals discussed above. Hence, the DRIFTS spectra support the presence of formate species on the Co_5Ga_3 catalyst. The second expected formate peak[23] near 1380 cm^{-1} was not observed; however, this peak cannot be ruled out due to the low signal to noise at this frequency. For the Co catalyst, formate features were not detected; however, the presence of H_2O (due to the hydrogenation of CO_2 to CH_4) may have obscured a weak formate feature.

In addition to formate species, chemisorbed CO species were observed. Based on our calculations, methanol formation occurs via formate, and we expect the chemisorbed CO species to act as spectators in the case of Co_5Ga_3 with the CO formed through reverse water gas shift. For both Co and Co_5Ga_3, a peak was observed at 2009 cm^{-1}. This peak agrees well with the expected location for CO on a Co site.[25] The Co catalyst's peak was much broader than that of the Co_5Ga_3 catalyst. The Co catalyst peak was asymmetric and skewed towards lower frequencies. These lower frequencies may correspond to CO on bridging sites. An additional peak at 1877 cm^{-1} was observed on the Co_5Ga_3 catalyst that can be assigned to CO adsorbed at threefold sites.[26]

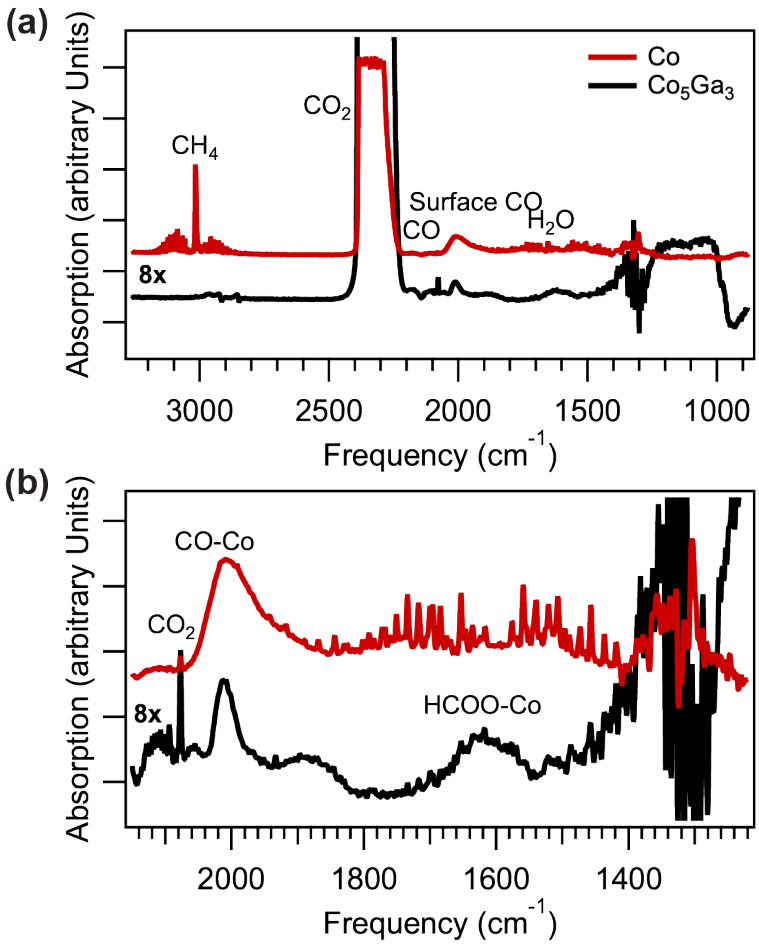

Figure 7. DRIFTS of Co and Co_5Ga_3 catalysts at 250 °C in 9 bar 3:1 CO_2:H_2. (b) is the surface CO and formate region of (a).

Through DFT calculations and microkinetic modelling, we predicted a new CoGa methanol synthesis catalyst. Our calculations indicated that the hydrogenation of CO_2 to methanol proceeds via a formate intermediate. Our experimental results proved that CoGa is indeed a highly selective catalyst for methanol during CO_2 hydrogenation in agreement with our predictions. Using *in-situ* DRIFTS we verified that surface formate species were present, in line with our proposed mechanism.

Conclusions

Although not fully optimized, CoGa catalysts showed promising selectivity for the hydrogenation of CO_2 to methanol. DFT was used to investigate the pathway for CO_2 hydrogenation and explain the selectivity of CoGa catalysts for methanol. The performance of the catalysts was sensitive to the CoGa ratio with increasing Ga content resulting in increased dimethyl ether selectivity and increasing Co content increasing selectivity towards methane. The product selectivity of the prepared catalysts closely

matched our DFT predictions. The prepared catalysts, although lower in performance than a commercial CuZn methanol synthesis catalyst, are comparable in selectivity. With additional optimization, the performance of CoGa methanol syntheses catalysts may exceed that of current state-of-the-art catalysts.

Acknowledgments

We acknowledge financial support from the U.S. Department of Energy, Office of Basic Energy Sciences to the SUNCAT Center for Interface Science and Catalysis. The authors gratefully acknowledge the use of the Stanford Nano Shared Facilities (SNSF) of Stanford University for sample characterization. The authors would like to thank Andrew Riscoe for performing the nitrogen physisorption measurements. Ang Cao gratefully acknowledges financial support from China Scholarship Council.

References

(1) Olah, G. A.; Goeppert, A.; Prakash, G. K. S. Chemical Recycling of Carbon Dioxide to Methanol and Dimethyl Ether: From Greenhouse Gas to Renewable, Environmentally Carbon Neutral Fuels and Synthetic Hydrocarbons. *J. Org. Chem.* **2009**, *74*, 487–498.

(2) Schumann, J.; Lunkenbein, T.; Tarasov, A.; Thomas, N.; Schlögl, R.; Behrens, M. Synthesis and Characterisation of a Highly Active Cu/ZnO:Al Catalyst. *ChemCatChem* **2014**, *6*, 2889–2897.

(3) Sharafutdinov, I.; Elkjær, C. F.; De Carvalho, H. W. P.; Gardini, D.; Chiarello, G. L.; Damsgaard, C. D.; Wagner, J. B.; Grunwaldt, J. D.; Dahl, S.; Chorkendorff, I. Intermetallic Compounds of Ni and Ga as Catalysts for the Synthesis of Methanol. *J. Catal.* **2014**, *320*, 77–88.

(4) Studt, F.; Sharafutdinov, I.; Abild-Pedersen, F.; Elkjær, C. F.; Hummelshøj, J. S.; Dahl, S.; Chorkendorff, I.; Nørskov, J. K. Discovery of a Ni-Ga Catalyst for Carbon Dioxide Reduction to Methanol. *Nat. Chem.* **2014**, *6*, 320–324.

(5) Fujitani, T.; Saito, M.; Kanai, Y.; Takeuchi, M.; Moriya, K.; Watanabe, T.; Kawai, M.; Kakumoto, T. Methanol Synthesis from CO 2 and H 2 over Cu/ZnO/Ga 2 O 3 Catalyst. *Chem. Lett.* **1993**, *22*, 1079–1080.

(6) Toyir, J.; Ramírez de la Piscina, P.; Fierro, J. L. G.; Homs, N. Catalytic Performance for CO2 Conversion to Methanol of Gallium-Promoted Copper-Based Catalysts: Influence of Metallic Precursors. *Appl. Catal. B Environ.* **2001**, *34*, 255–266.

(7) Ning, X.; An, Z.; He, J. Remarkably Efficient CoGa Catalyst with Uniformly Dispersed and Trapped Structure for Ethanol and Higher Alcohol Synthesis from Syngas. *J. Catal.* **2016**, *340*, 236–247.

(8) An, Z.; Ning, X.; He, J. Ga-Promoted CO Insertion and C–C Coupling on Co Catalysts for the Synthesis of Ethanol and Higher Alcohols from Syngas. *J. Catal.* **2017**, *356*, 157–164.

(9) Giannozzi, P.; Baroni, S.; Bonini, N.; Calandra, M.; Car, R.; Cavazzoni, C.; Ceresoli, D.; Chiarotti, G. L.; Cococcioni, M.; Dabo, I.; et al. QUANTUM ESPRESSO: A Modular and Open-Source Software Project for Quantum Simulations of Materials. *J. Phys. Condens. Matter* **2009**, *21*, 395502.

(10) Bahn, S. R.; Jacobsen, K. W. An Object-Oriented Scripting Interface to a Legacy Electronic Structure Code. *Comput. Sci. Eng.* **2002**, *4*, 56–66.

(11) Wellendorff, J.; Lundgaard, K. T.; Møgelhøj, A.; Petzold, V.; Landis, D. D.; Nørskov, J. K.; Bligaard, T.; Jacobsen, K. W. Density Functionals for Surface Science: Exchange-Correlation Model Development with Bayesian Error Estimation. *Phys. Rev. B - Condens. Matter Mater. Phys.* **2012**, *85*, 32–34.

(12) Wellendorff, J.; Silbaugh, T. L.; Garcia-Pintos, D.; Nørskov, J. K.; Bligaard, T.; Studt, F.; Campbell, C. T. A Benchmark Database for Adsorption Bond Energies to Transition Metal Surfaces and Comparison to Selected DFT Functionals. *Surf. Sci.* **2015**, *640*, 36–44.

(13) Henkelman, G.; Uberuaga, B. P.; Jónsson, H. Climbing Image Nudged Elastic Band Method for Finding Saddle Points and Minimum Energy Paths. *J. Chem. Phys.* **2000**, *113*, 9901–9904.

(14) Medford, A. J.; Shi, C.; Hoffmann, M. J.; Lausche, A. C.; Fitzgibbon, S. R.; Bligaard, T.; Nørskov, J. K. CatMAP: A Software Package for Descriptor-Based Microkinetic Mapping of Catalytic Trends. *Catal. Letters* **2015**, *145*, 794–807.

(15) Lausche, A. C.; Medford, A. J.; Khan, T. S.; Xu, Y.; Bligaard, T.; Abild-Pedersen, F.; Nørskov, J. K.; Studt, F. On the Effect of Coverage-Dependent Adsorbate-Adsorbate Interactions for CO Methanation on Transition Metal Surfaces. *J. Catal.* **2013**, *307*, 275–282.

(16) Schumann, J.; Medford, A. J.; Yoo, J. S.; Zhao, Z.-J.; Bothra, P.; Cao, A.; Studt, F.; Abild-Pedersen, F.; Nørskov, J. K. Selectivity of Synthesis Gas Conversion to C2+ Oxygenates on Fcc(111) Transition-Metal Surfaces. *ACS Catal.* **2018**, *8*, 3447–3453.

(17) Medford, A. J.; Lausche, A. C.; Abild-Pedersen, F.; Temel, B.; Schjødt, N. C.; Nørskov, J. K.; Studt, F. Activity and Selectivity Trends in Synthesis Gas Conversion to Higher Alcohols. *Top. Catal.* **2014**, *57*, 135–142.

(18) Singh, J. A.; Yang, N.; Liu, X.; Tsai, C.; Stone, K. H.; Johnson, B.; Koh, A. L.; Bent, S. F. Understanding the Active Sites of CO Hydrogenation on Pt–Co Catalysts Prepared Using Atomic Layer Deposition. *J. Phys. Chem. C* **2018**, *122*, 2184–2194.

(19) Abild-Pedersen, F.; Greeley, J.; Studt, F.; Rossmeisl, J.; Munter, T. R.; Moses, P. G.; Skúlason, E.; Bligaard, T.; Nørskov, J. K. Scaling Properties of Adsorption Energies for Hydrogen-Containing Molecules on Transition-Metal Surfaces. *Phys. Rev. Lett.* **2007**, *99*, 016105.

(20) Studt, F.; Behrens, M.; Kunkes, E. L.; Thomas, N.; Zander, S.; Tarasov, A.; Schumann, J.; Frei, E.; Varley, J. B.; Abild-Pedersen, F.; et al. The Mechanism of CO and CO2 Hydrogenation to Methanol over Cu-Based Catalysts. *ChemCatChem* **2015**, *7*, 1105–1111.

(21) Petre, A.; Auroux, A.; Gélin, P.; Caldararu, M.; Ionescu, N. Acid–base Properties of Supported Gallium Oxide Catalysts. *Thermochim. Acta* **2001**, *379*, 177–185.

(22) Zhang, Y.; Jacobs, G.; Sparks, D. E.; Dry, M. E.; Davis, B. H. CO and CO2 Hydrogenation Study on Supported Cobalt Fischer-Tropsch Synthesis Catalysts. *Catal. Today* **2002**, *71*, 411–418.

(23) Das, T.; Deo, G. Synthesis, Characterization and in Situ DRIFTS during the CO2 Hydrogenation Reaction over Supported Cobalt Catalysts. *J. Mol. Catal. A Chem.* **2011**, *350*, 75–82.

(24) Fisher, I. A.; Bell, A. T. In Situ Infrared Study of Methanol Synthesis from H2/CO over Cu/SiO2 and

Cu/ZrO2/SiO2. *J. Catal.* **1998**, *178*, 153–173.

(25) Toomes, R. L.; King, D. A. The Adsorption of CO on Co{1010}. *Surf. Sci.* **1996**, *349*, 1–18.

(26) Weststrate, C. J.; van de Loosdrecht, J.; Niemantsverdriet, J. W. Spectroscopic Insights into Cobalt-Catalyzed Fischer-Tropsch Synthesis: A Review of the Carbon Monoxide Interaction with Single Crystalline Surfaces of Cobalt. *J. Catal.* **2016**, *342*, 1–16.

Supporting information

Table S1. All possible elementary reactions involved in the formation of CO, CH3OH and CO from CO_2 hydrogenation together with the reaction energies (ΔE) and activation energies (E_a) on Co_1Ga_1 (110) surface.

Elementary reaction		ΔE (eV)	E_a (eV)
$CO_2 + H \rightarrow HCOO$	R1-1	-0.51	0.56
$CO_2 + H \rightarrow COOH$	R1-2	0.12	1.72
$CO_2 \rightarrow CO + O$	R1-3	-0.09	1.02
$COOH + H \rightarrow CO + OH$	R2-1	-0.53	0.25
$HCOO + H \rightarrow HCO + OH$	R3-1	0.45	0.74
$HCOO + H \rightarrow HCOOH$	R3-2	0.51	1.07
$HCOOH + H \rightarrow H_2COOH$	R4-1	-0.02	1.55
$H_2COOH \rightarrow H_2CO + OH$	R5-1	0.39	0.42
$HCO + H \rightarrow CHOH$	R6-1	0.11	0.79
$HCO + H \rightarrow CH_2O$	R6-2	0.02	0.66
$CH_2O + H \rightarrow CH_2OH$	R7-1	-0.13	1.20
$CH_2O + H \rightarrow CH_3O$	R7-2	-0.63	0.47
$CH_3O + H \rightarrow CH_3 + OH$	R8-1	-0.08	1.40
$CH_3O + H \rightarrow CH_3OH$	R8-2	-0.33	0.75
$CH_3 + H \rightarrow CH_4$	R9-1	-0.99	0.50

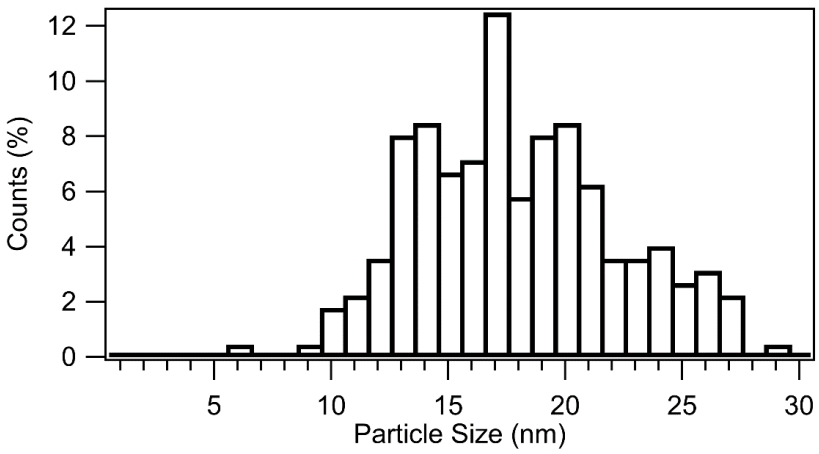

Figure S1. Particle size distribution of Co_5Ga_3 catalyst measured using TEM.